Microwave Properties of an Inhomogeneous Optically Illuminated Plasma in a Microstrip Gap

C. D. Gamlath, *Student Member, IEEE*, D.M. Benton, and M.J. Cryan, *Senior Member, IEEE*

***Abstract*— The optical illumination of a microstrip gap on a thick semiconductor substrate creates an inhomogeneous electron-hole plasma in the gap region. This allows the study of the propagation mechanism through the plasma region. This paper uses a multilayer plasma model to explain the origin of high losses in such structures. Measured results are shown up to 50 GHz and show good agreement with the simulated multilayer model. The model also allows the estimation of certain key parameters of the plasma such as carrier density and diffusion length which are difficult to measure by direct means. The detailed model validation performed here will enable the design of more complex microwave structures based on this architecture. While this paper focuses on monocrystalline silicon as the substrate, the model is easily adaptable to other semiconductor materials such as GaAs.**

***Index Terms*—Microwave photonics, propagation in complex media, plasmas, RF microwave photonic devices, Silicon.**

I. Introduction

Optically illuminated plasmas in silicon have found use in numerous applications. Some of these include plasma antennas, tuneable frequency selective surfaces (FSS), generation of millimetre wave pulses, beam scanning antennas and tuneable phase shifters [1,2,3]. Millimetre wave tuneable phase shifters have been investigated using both and microstrip [3,4] and waveguide [4,5] architectures. The success in designing such devices for practical applications depends on accurately simulating the microwave properties of the optically illuminated plasma. The modelling and measurement of the effects of optical illumination on the reflection characteristics of microstrip discontinuities is shown in [6,7]. Investigations of the phase shift properties of microstrip and coplanar gaps up to 12 GHz have also been shown [3]. Much of this work has focused on using small regions of the plasma of the order of 10s of microns. The illumination is usually fed from the end of a multimode fibre and the illumination areas are much smaller than the shortest microwave wavelength. The effect of the electron-hole plasma is then localized and lumped element modelling is usually sufficient to account for the plasma effects.

This paper attempts to extend these concepts to longer lengths of plasma which are significant fractions of the microwave wavelength. Here lumped element modelling is no longer valid and propagation through the plasma must be considered. Although such propagation effects have been considered for waveguide structures [4], we believe this is the first such study for microstrip circuits. This paper presents measured and modelled results for illumination of a microstrip gap from DC up to 50 GHz. The microstrip lines on either end of the gap were fabricated directly on the silicon substrate. In some of our previous works we have tried to couple the illuminated plasma region to microstrip lines on Duroid [8] and have found this to be an inefficient method of coupling to the plasma. The motivation for this work is to aid in the development of a microstrip architecture that can effectively transmit microwave frequencies across long lengths of plasma. We expect such structures will enable the development of novel tuning methods based on spatially varying plasma regions [9].

Starting with a model similar to [7], it is shown that for the case of the gap a ten layer model is sufficient for good agreement with measured results. After this a comparison between the simulated and measured results allows the key parameters of the plasma to be identified. Section II describes the theoretical basis for the modelling of photoconductivity in semiconductors. This is followed by a detailed description of the measurements in section III and then an analysis of the simulated results in section IV, followed by the concluding remarks.

II. Photoconductivity in Semiconductors

A. Carrier Generation and Recombination

When an intrinsic semiconductor wafer is illuminated with photon energy just above its bandgap (1.1 eV for silicon), a significant portion of the absorbed photon energy goes into exciting electrons from the valence band into the conduction band. This provides an excess density of free electrons and holes available for conduction thus forming a plasma layer. The presence of these charge carriers also changes the permittivity of the area under illumination.

If the illumination power is held constant, a quasi-steady state is reached where the average excess carrier density can be assumed constant. The conducting layer thus formed has a carrier density which decays exponentially with depth. The point at which the illumination intensity drops to $1/e$ of its surface value is given by the absorption depth $1/\alpha$, where α is the absorption coefficient and is a function of illumination wavelength. The reciprocal of the absorption coefficient is known as the absorption depth.

Manuscript received June 9, 2014; revised August 14, 2014. The funding for this project is provided through an EPSRC grant and supported by L3-TRL Technologies U.K.

C.D. Gamlath and M.J. Cryan are with the Department of Electrical and Electronic Engineering, University of Bristol, Bristol, BS81TR, U.K. (email: chris.gamlath@bristol.ac.uk; m.cryan@bristol.ac.uk).

D. M. Benton is with the Aston Institute of Photonics Technologies, Aston University, Aston Triangle, Birmingham, B47ET, U.K. (email: d.benton@aston.ac.uk).

The generation of excess carriers due to illumination causes recombination within the semiconductor since the excess have only a finite lifetime. There is also the effect of diffusion which becomes significant when the absorption depth is much less than the diffusion length. When the generation rate, *G(z)*, is held constant and quasi-steady state conditions are reached, the spatial distribution of charges becomes constant with time. The generation rate is given by (1) below.

$$G(z) = \frac{q_e \alpha I_0 (1 - \Gamma_s) e^{-\alpha z}}{h\nu} \quad (1)$$

where q_e is a constant representing the combined effect of quantum efficiency and carrier generation efficiency. α is absorption coefficient, z is depth from the semiconductor surface, I_0 is illumination intensity at the semiconductor surface, Γ_s is surface reflectance and $h\nu$ is the photon energy (1.5 eV for 830 nm illumination). The wavelength of 830 nm was chosen to be close to the optimum carrier generation efficiency for silicon. The recombination rate under steady state, assuming that the Auger effects are negligible is given by:

$$R(z, n_{ex}) = \frac{n_{ex}}{\tau} \quad (2)$$

where n_{ex} represents the excess amount of charges generated by illumination and τ is recombination time for the bulk semiconductor. Using the general equations of continuity and charge neutrality [10] and setting the induced field to zero, it is possible to derive the following equation for the excess carriers within the semiconductor:

$$\frac{\partial n_{ex}}{\partial t} = G(z) - R(z, n_{ex}) + D_n \frac{\partial^2 n_{ex}}{\partial z^2} \quad (3)$$

where $D_n = {L_n^2}/{\tau}$ is the ambipolar diffusion constant for bulk silicon and L_n is the diffusion length. Setting $\frac{\partial n_{ex}}{\partial t} = 0$ which is valid at equilibrium gives, after some rearranging gives:

$$L_n^2 \frac{\partial^2 n_{ex}}{\partial z^2} - n_{ex} = \frac{-\tau\, q_e \alpha I_0 (1 - \Gamma_s) e^{-\alpha z}}{h\nu} \quad (4)$$

Note that this equation was derived for one dimension. The generalization to three dimensions can be obtained by changing the second differential in the first term to a Laplacian. The one dimensional analysis is sufficient for the gap structure considered in this paper since there is a nearly even illumination intensity across the entire gap region.

Two boundary conditions are specified for (4), one at the surface and the other at an infinite distance from the surface. The first condition is given by (5) below:

$$\frac{dn_{ex}(0)}{dz} = \tau S \frac{n_{ex}(0)}{L_n^2} \quad (5)$$

where $n_{ex}(0)$ is the excess carrier density at the surface and S is surface recombination velocity. The second condition is given by:

$$n_{ex}(\infty) = 0 \quad (6)$$

Note that this latter condition at $z = \infty$ is valid only when the thickness of the semiconductor substrate is a few times greater than the diffusion length such that the concentration levels at the bottom of the semiconductor have dropped to nearly zero. Solving (4) subject to these boundary conditions gives:

$$n_{ex} = \frac{-\tau\, q_e \alpha I_0}{h\nu(\alpha^2 L_n^2 - 1)} \left\{ e^{-\alpha z} - \frac{\alpha L_n + {\tau S}/{L_n}}{1 + {\tau S}/{L_n}} e^{-z/L_n} \right\} \quad (7)$$

where the diffusion length is much greater than the absorption depth $L_n \gg 1/\alpha$ (as in our case) the above equation approximates to the following as z moves away from the surface:

$$n_{ex} = \frac{\tau\, q_e I_0}{h\nu(L_n + \tau S)} \left\{ e^{-z/L_n} \right\} \quad (8)$$

This shows that the exponential tail of carriers into the semiconductor is determined entirely by the ambipolar diffusion within the semiconductor. Typical values of L_n, τ and S are in the ranges of 100 to 150 μm, 0.1 to 10 μs and 10^2 to 10^5 cm/s respectively [11]. Applying (8) to a typical sample of silicon shows that if the bulk recombination time is long (above 1 μs) and surface recombination is high, then $\tau S \gg L_n$ and the excess carrier concentration is limited almost entirely by surface recombination. This highlights the importance of a passivated surface to reduce the surface recombination velocity.

For a known carrier concentration, the conductivity of the plasma can be calculated using (9) below

$$\sigma = e(n_{ex} + n_o)(\mu_e + \mu_h) \quad (9)$$

where σ is conductivity (S/cm), e is the electron charge (Coulombs), n_0 is intrinsic carrier concentration (/cm^3), μ_e and μ_h are the electron and hole mobilities (1350 and 480 cm^2/Vs for intrinsic silicon). Fig. 1 shows the exponential decay of conductivity with depth for various illumination intensities at a wavelength of 830 nm (where $1/\alpha$ = 15 μm).

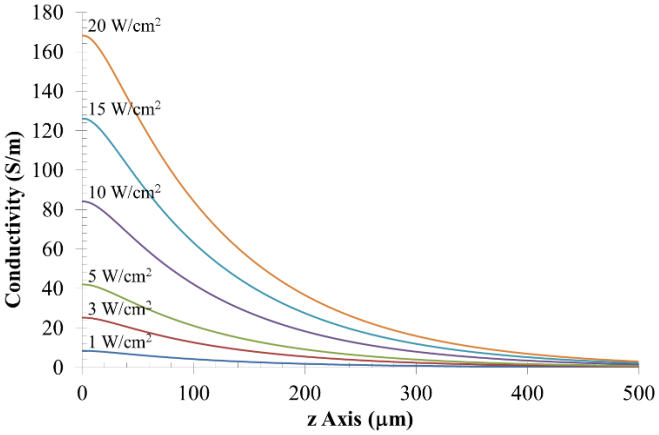

Fig. 1. Conductivity vs. substrate depth for silicon. (The figures on top of each line indicate illumination intensity in W/cm^2).

The surface recombination velocity was taken as 10^3 cm/s and the bulk recombination time as 1 µs, these are common values found in most practical processes [12].

As well as increasing the conductivity, a second effect caused by the induced carriers is to decrease the real part of the permittivity. This can be calculated using the formula below:

$$\varepsilon_{re} = \varepsilon_{si}\left(1 - \frac{\omega_p^2 \chi^2}{1+\omega^2 \chi^2}\right) \quad (10)$$

where ε_{si} is the dielectric permittivity of silicon, ω_p is the plasma frequency and χ is the carrier collision time which is related to carrier mobility by the equation below:

$$\chi = \frac{m^*}{e}\mu \quad (11)$$

where μ is the carrier mobility, m^* is effective electron mass and e is electron charge. ω_p in (10) is given by:

$$\omega_p = \sqrt{\frac{Ne^2}{m^* \varepsilon_{si}}} \quad (12)$$

where N is carrier concentration. At high carrier concentration levels the real part of permittivity (10) can take negative values. However for frequencies well below the plasma frequency, such as those studied in this paper, the effect of the conductivity tends to dominate the response and the real part of permittivity becomes less significant. Table I shows several values for various illumination intensities.

The conductivity profile derived in this section is used for building the simulation model of section IV and the conductivity values calculated in Table I are compared with those obtained from S parameter measurements. In this section we have introduced the basic physics of the illuminated gap, the following section will show measured results in both the DC and microwave regimes.

Optical Intensity (W/cm^2)	**Carrier Concentration (/cm^3)**	**Conductivity (S/m)**	**Dielectric Constant**
0	1.45 x10^{10}	4.25 x10^{-4}	11.9
0.5	1.43 x10^{14}	4.2	11.8
1	2.90 x10^{14}	8.4	11.7
5	1.43 x10^{15}	42	10.9
10	2.87 x10^{15}	84	10.0
15	4.30 x10^{15}	126	9.0
20	5.73 x10^{15}	168	8.0

TABLE I: Carrier concentration, conductivity and permittivity for different levels of optical intensity.

III. Measurement

A. *Measurement Setup and Calibration*

This section describes in detail the test setup used for measurements along with the initial calibration. A schematic of the test structure is shown in Fig. 2a along with a picture of the actual device in Fig.. 2b. The silicon substrate we have used is a lightly doped (Resistivity > 5 kΩ.cm), n-type, float zone wafer with a <100> orientation, a thickness of 500 µm and a polished top surface.

The microstrip lines were formed as follows. The silicon wafer was cleaned and dipped in a hydrofluoric acid solution for a two minutes. This was to remove any residual oxide from the surface of the wafer. Immediately after the etch the wafers were dried in a 90degC oven and sputter coated with 10 nm of titanium and 400 nm of gold. The 10 nm titanium layer was used to provide better adhesion of the gold. Both metals were deposited using a sputter coater with an ambient argon atmosphere. The wafer was then spin coated using a Microposit S1805-G2 photoresist. The photoresist was exposed under UV and developed using an MF-319 developer. The gold was etched using a TFA gold etching solution. The titanium adhesion layer was removed in a separate step using a titanium etchant for 3 minutes.

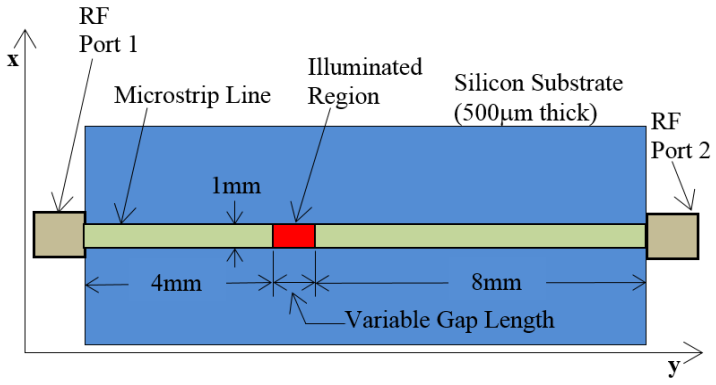

Fig. 2(a). Test circuit used for measurements.

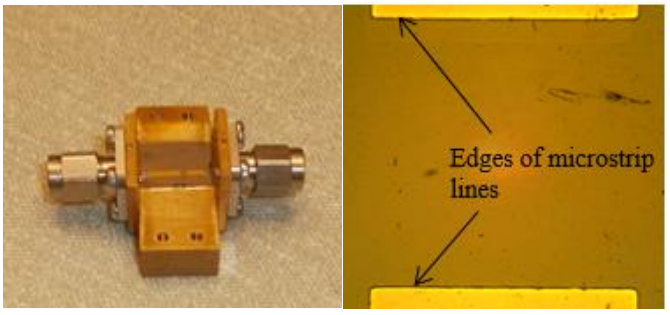

Fig. 2(b). Test Circuit (left) and magnified view of microstrip gap (right).

The RF to Microstrip transitions used for Port1 and Port2 were Anritsu K104M K-Type coax to Microstrip connectors. A 50 Ω line width is calculated to be 0.4 mm, however, this was not ideal for the illumination spot size used here and a compromise width of 1 mm has been used instead which has a line impedance of 30 Ω. The measured S parameters for a 1 mm width microstrip line are shown in Fig. 3. This shows less than 3dB of insertion loss up to 40 GHz and a reflection coefficient less than -10dB. Since the insertion loss through the plasma (of about 20dB) is much higher than the insertion loss

of 3dB the effect of the microstrip lines and coax transitions have a negligible impact on the final results.

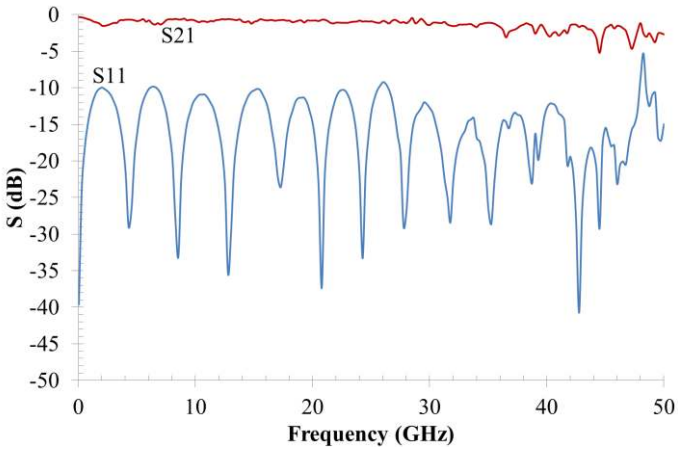

Fig. 3. S parameter response of a microstrip line of 1 mm width on silicon.

A schematic of the setup used for illumination is shown in Fig. 4a along with a picture of the setup in Fig. 4b. The laser diode was a 1W, 830 nm edge emitting laser with an emitting area of 50 x 5 μm^2.

The large facet size makes it difficult to collimate the laser output using standard optics.

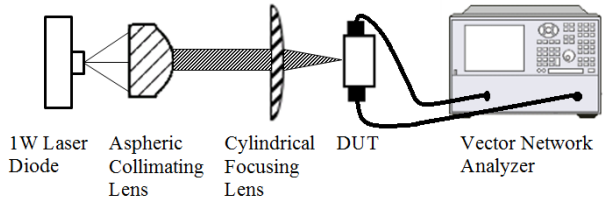

Fig. 4(a). Schematic of the optical setup.

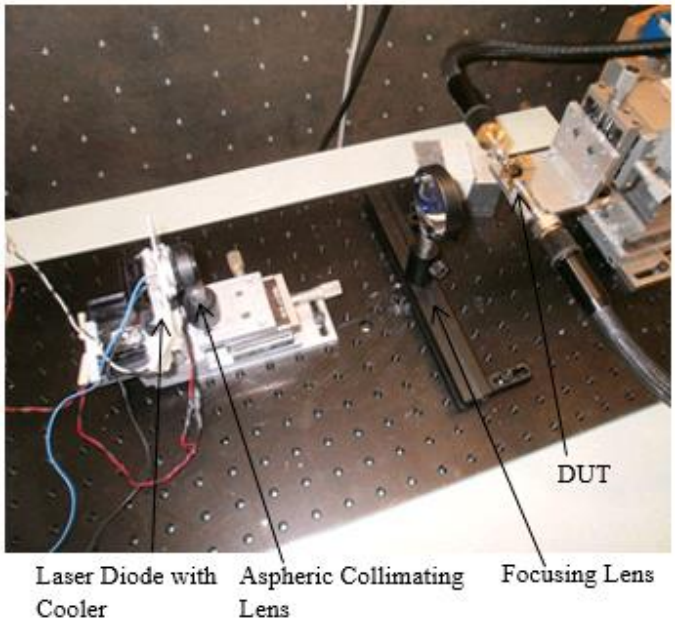

Fig. 4(b). Picture of the optical setup.

The Thorlabs C390TME-B aspheric collimating lens was found to give a good compromise between beam divergence angle and low loss. A 3-Axis Micrometre Stage was used for aligning the axis of the lens with centre of the laser diode. A cylindrical lens (Thorlabs LJ1695RM-B) was used to contract the fast axis of the laser diode while keeping the slow axis the same. This enabled a spot size of 2 mm x 1 mm to be obtained. The positioning of the cylindrical lens was less critical and used a standard optical mount. Using this method a maximum optical intensity of
16 W/cm^2 was obtained almost uniformly over a
2 x 1 mm^2 area.

B. DC Measurements

This section describes the DC characteristics of the plasma and shows measured results of the I-V curves across the illuminated gap. The DC circuit model for the gap is shown in Fig. 5. The two diodes represent the rectifying Schottky contacts between the metal lines and bulk silicon at either side of the gap. The distribution of the plasma near the ends of the gap is determined by whether this contact is ohmic or rectifying due to the depletion region effects [13]. In this case it was found to be a rectifying contact. The silicon substrate used was a lightly doped n-type with a resistivity greater than 5 kΩ.cm. This was required in order to keep the microwave substrate losses to a low level. Since one of the metal-semiconductor contacts will always be reverse biased, the reverse leakage current dominates the response at high illumination powers when the bulk resistance drops to well below its intrinsic value.

Fig. 5. DC model for the gap.

The DC measurements of the microstrip gap are shown in Fig. 6. The nonlinear effect of the Schottky diodes can be seen in both the dark and illuminated cases.

Due to the back-to-back rectifying contacts it is difficult to determine the DC properties of the plasma directly from the I-V curves. The next section describes a method for determining the plasma conductivity using microwave measurements.

C. Microwave Measurements

This section shows the measured data for the S parameters across the gap at varying illumination intensities. The S_{21} magnitude for a 1 mm gap under varying illumination levels is shown in Fig. 7. The graph shows a clear pattern in that the transmission at the lower frequencies increases significantly with increasing illumination intensity. At low frequencies the response is mainly resistive and we can use this data to determine the conductivity more accurately than in the case of DC measurements.

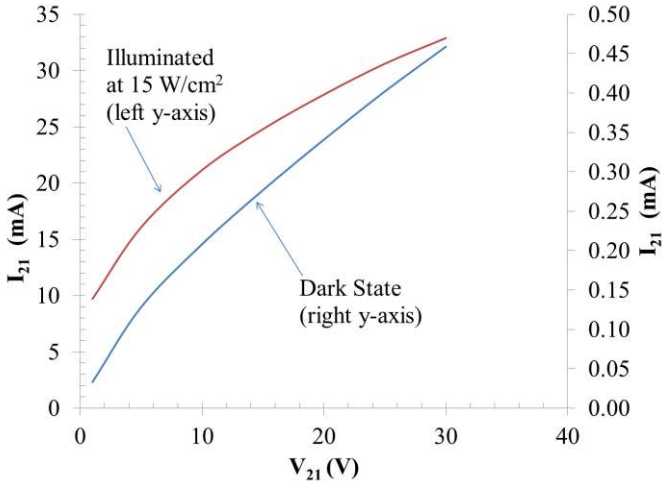

Fig. 6. Current across the gap (I21) vs. voltage (V21).

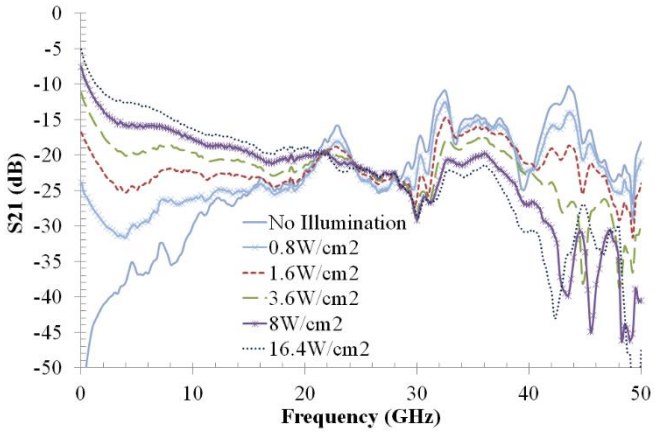

Fig. 7. Measured S21 magnitude for a 1 mm gap at varying illumination levels.

Using the S parameter measurements at 45 MHz the resistance across the gap can be calculated using the following formula [14].

$$S_{11} = \frac{R}{R + 2Z_0} \tag{13}$$

where R is the resistance in the gap and Z_0 is the characteristic impedance of the Vector Network Analyzer (VNA). Note that (13) is only valid in the low frequency limit (around 45 MHz) where the plasma can be approximated as a lumped element circuit. The resistance is converted into a conductivity using the length of the gap and the thickness of the plasma. A good approximation for the thickness is the point where the carrier concentration drops to 1/*e* of its surface value (approximately 120µm for our silicon sample). The conductivity obtained using this method is shown in Fig. 8. This value of conductivity is within 25% of the calculated values in Table 1 of Section II. Note that in the calculation of (13), we have assumed the effect of series capacitance at the metal-plasma junction to be negligible at 45 MHz.

One important feature in Fig. 8 is that the upper end of the graph has a positive slope at high illumination intensities. This indicates that still higher conductivities can be achieved by further increases in illumination intensity. From a practical point of view this means that losses can be further reduced by increasing illumination intensity. Losses in plasma tuned circuits are one of their main challenges. The loss can be calculated directly by measuring the reflection coefficient and combining this with the transmission coefficient as explained below. The measured reflection coefficient (S_{11}) is shown in Fig. 9. This shows that the plasma is matched reasonably well to the line at high illumination levels. At frequencies above 20 GHz, resonant peaks can be seen in the S_{21} results. At these frequencies, the two microstrip lines are resonantly coupled to the plasma region.

$$Absorption\ Loss = 1 - |S_{11}|^2 - |S_{21}|^2 \tag{14}$$

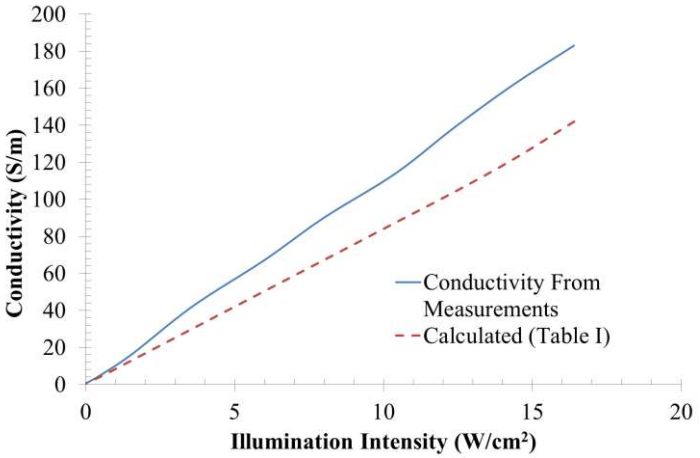

Fig. 8. Conductivity vs. illumination intensity derived from S parameter measurements at 45 MHz.

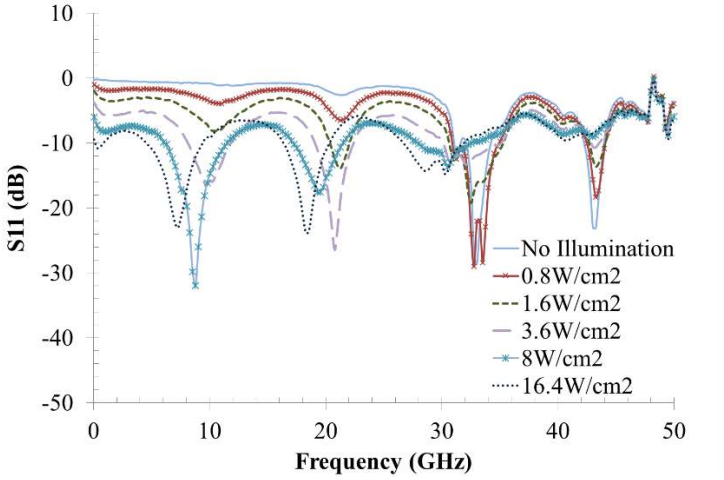

Fig. 9. Measured S11 magnitude for a 1 mm gap at varying illumination levels.

Using the data from Figs. 7 and 9 shows that for frequencies beyond 2 GHz nearly 90% of the transmitted power is lost due to absorption in the plasma. The models developed in this paper will be used to minimise these losses and several practical methods for doing this are currently being investigated, these are discussed in the conclusion.

The variations in the frequency shift with illumination intensity seen in the S_{11} response is mainly due to the changes in the fringing capacitance at the end of the line caused by the plasma [15]. The value of this capacitance is highly dependent on the diffusion profile of the plasma. This has been fully included in the numerical modelling presented later in this paper. Fig. 10 shows the measured phase shift for various illumination levels. The phase shift is plotted relative to the dark state. An almost constant phase shift of about 100degrees was observed from the frequency range between 1 and 20 GHz. Beyond this the phase shift shows a more rapid variation. The reasons for this phase characteristic are explained in section IV. The microstrip gap structure presented here has not been optimized for phase shift applications, a more optimum structure is the interdigitated gap structure as shown in [16].

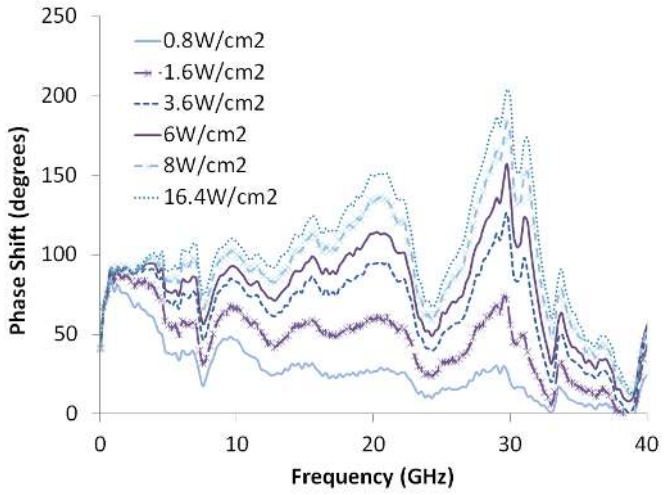

Fig. 10. Measured S21 phase shift for a 1 mm gap at varying illumination levels.

The measured results presented here are compared with the simulation model in the next section. An analysis of the field profiles within the plasma is also presented.

IV. Simulation and Analysis

A. Introduction

The results of the previous section were analysed with the help of simulations carried out using CST™ Microwave Studio's transient solver. This uses a finite integration technique (FIT) for solving Maxwell's equations in a 3D space. The two models used for the analysis are shown in Fig. 11. Fig. 11a shows the single layer and Fig. 11b shows the multilayer model which accounts for the diffusion of the carriers in all three dimensions as described in section II. The optimum number of layers required was found by gradually decreasing the layer count from 30 to 5 and observing the changes to the results in each case. This was to get the best fit of the measured data using the least number of layers. A ten layer model was found to be sufficient. The conductivity of each layer was calculated by combining (8) and (9) of section II. The permittivity of each layer was set according to Table 1 of Section II. The rectangular nature of this model is an approximation which was adopted due to its simplicity. A more accurate model would require the solution of (4) in three dimensions which results in a curved profile for the plasma and increases simulation overhead. Fig. 11c shows a 2D version of Fig. 11b where some of the detail can be seen more clearly. The dimensions of the microstrip lines and silicon substrate are shown in Fig. 2.

The single layer model of Fig. 11a is used for investigating the effect of confining the carriers to a single layer just below the silicon surface. By comparing the differences in S_{21} between the two models the effect of the diffusion tail on the overall loss through the plasma can be identified. The thickness of the single layer model is taken as the depth where the illumination intensity drops to below 5% of its surface value. This is equivalent to three absorption depths and is about 50 μm for an illumination wavelength of 830 nm in silicon.

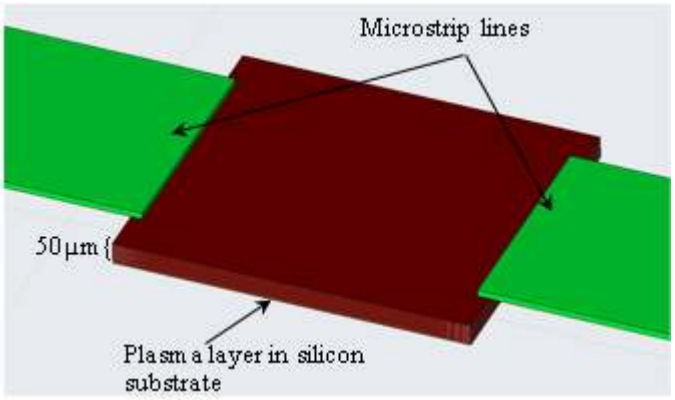

Fig. 11(a). Single layer model for the plasma.

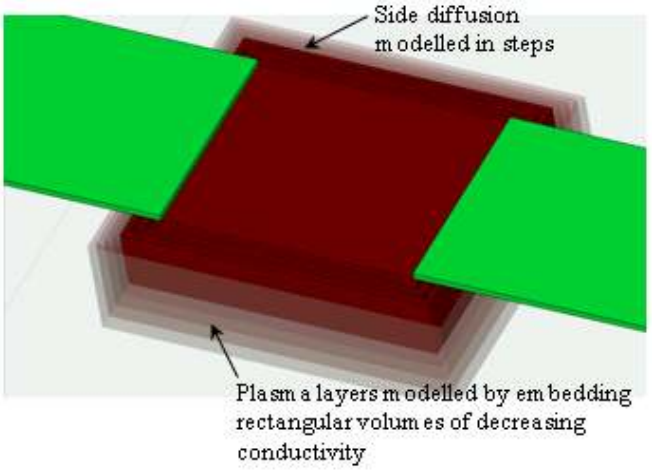

Fig. 11(b). Multilayer model of the plasma.

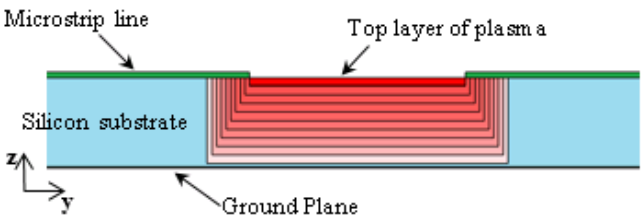

Fig. 11(c). Cross-sectional view of multilayer model.

B. Analysis Using S-Parameters

The results of the single layer and multilayer models are compared first. Fig. 12 shows the comparison of S_{21} for the two cases along with measured results. The conductivity of the top layer in each model (Fig. 11a, 11b) is kept constant. The single layer model is seen to improve the high frequency losses by at least 10dB. It highlights the important fact that a significant amount of the attenuation can be recovered by confining the plasma region to the substrate surface. The measured results show a close fit to the multilayer model and are within 3dB of the simulated results for frequencies below 20 GHz.

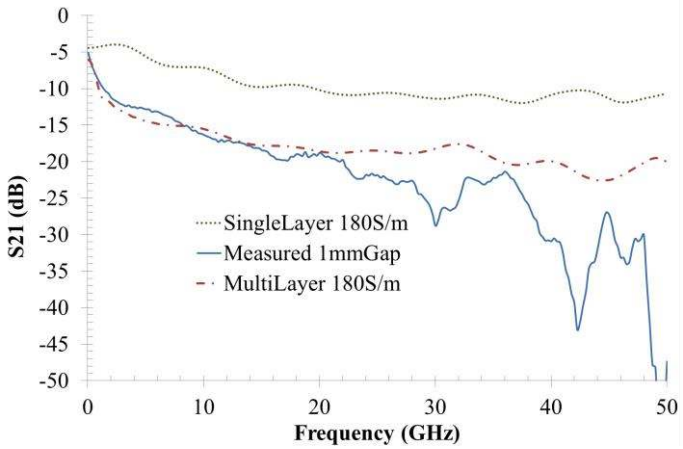

Fig. 12. Comparison of single and multilayer models with measured results for a 1 mm gap.

The effect of increasing the gap length is shown in Fig. 13 along with measured results. The simulated results have used the multilayer model of Fig. 11b with a top layer conductivity of 180 S/m which is equivalent to an illumination level of 16 W/cm^2(see Fig. 8). Fig. 13 shows that at frequencies below about 20 GHz the multilayer model (Fig. 11b) can accurately predict the effect of varying gap lengths. The inaccuracies in the simulated results above this frequency is thought to be due to approximations used in creating the multilayer model as stated in the introduction (Part A). Hence Fig. 13 shows the practical frequency limit of using rectangular sections to approximate the plasma profile. The illumination intensity was the same for both 1 mm and 1.5 mm cases. Since the optical beam had a near constant intensity across a 2 mm length, the microstrip lines on either side of the gap block the illumination outside of the gap region thus creating a near constant illumination intensity inside the gap.

The effects of line width mismatch were investigated through a series of simulations. The line width of 1 mm was chosen due to difficulties with focusing the high power laser, thus the minimum beam width achievable without considerable loss of optical power was 1 mm. The impedance of a 1 mm line on our sample of silicon was found to be 30 Ω while the line width required for a 50 Ω impedance was 0.4 mm.

The effects of mismatch loss between the two cases was investigated by varying the line and plasma widths individually. Figs. 14a and b show the S-parameter results for the four cases. Case 1 is the original gap line where both the line and plasma width are kept at 1 mm. Case 2 is where the line width was changed to 0.4 mm while the plasma width was kept at 1 mm. Case 3 shows both the plasma and line widths changed to 0.4 mm. Due to beam width restrictions this case is not practically viable but was investigated to complement the results of case 2. A transmission line taper from 50 Ω to 30 Ω was also investigated in case 4. The selected taper was based on a Dolph-Tchebycheff type design [17]. Simulations of the taper on its own showed a return loss of less than -20dB after

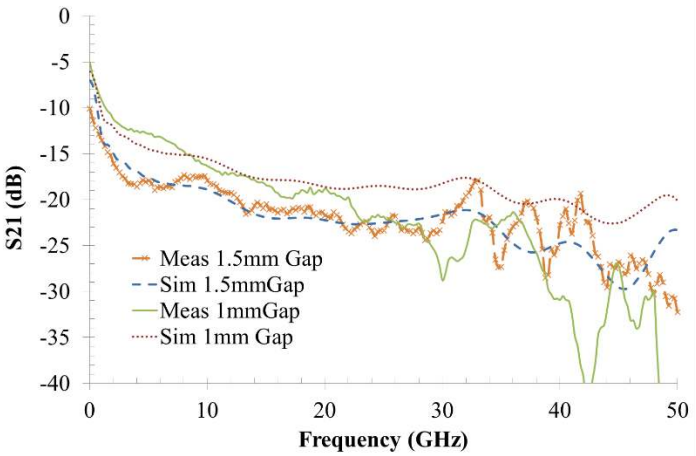

Fig. 13. Simulated and measured results for 1 mm and 1.5 mm gap lengths for 16 W/cm2 illumination.

5 GHz. The minimum frequency of 5 GHz was chosen in order to limit the length of the taper and hence keep simulation times to a reasonable level. The taper was then inserted in place of the microstrip lines on either side of the plasma. This allowed the two line sections to be matched to 50 Ω at the ports while keeping the line width at 1 mm next to the plasma. The multilayer conductivity profile of Fig. 11b was used across all four cases with a top conductivity of 180 S/m and a plasma length of 1 mm.

The results of Fig. 14a show that for case 1 (the original 1 mm case), the S_{11} results are within a few dB of the measured results of Fig. 9. This is for a 16 W/cm^2 illumination intensity. The 400µm lines of cases 2 and 3 provide a better match to 50 Ω than the original case as seen in the S_{11} results of Fig. 14a. The taper results of case 4 also show better overall matching to 50 Ω with the S_{11} being less than -10dB for frequencies above 5 GHz. The S_{21} results of Fig. 14b however show that cases 2 and 3 are on average about 3dB lower than cases 1 and 4. This is due to a DC resistive effect related to the size of the line with respect to the plasma. In cases 1 and 4 a 1x1 mm area plasma is fed by a 1 mm wide line. This results in near uniform current flow across the whole plasma. Whereas in cases 2 and 3 the DC resistance will be higher due to the plasma being fed by 0.4 mm lines hence resulting in a lower S_{21}. The increase in inductive effects due to the narrower lines are also accounted for in the numerical simulation but these are more difficult to interpret directly. Overall, these results shows that mismatch losses are relatively minor when compared to resistive losses in the plasma.

The effect of varying diffusion lengths is shown in Fig. 15. Minor changes in diffusion length of the order of 10s of microns were seen to cause significant changes in the S_{21} at 2 GHz and above. The close match between measured and simulated results in this frequency range could only be obtained

for a single diffusion length. This was found to be 120 μm which is within the range of values stated in literature (85 μm to 150 μm) [12]. Hence we were able to obtain a better estimate for the diffusion length of our silicon sample using the microwave measurements.

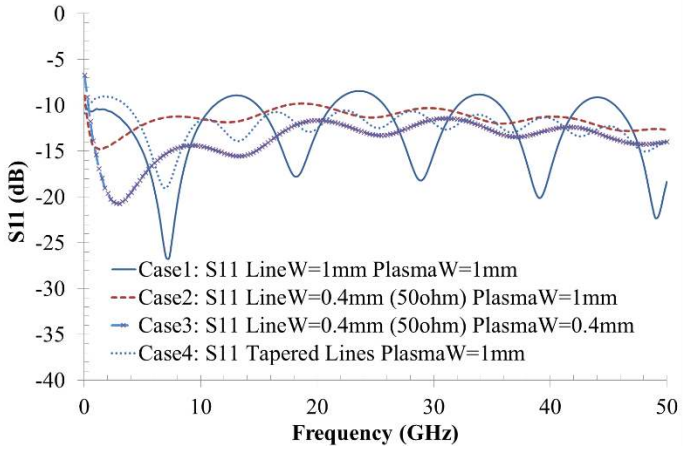

Fig. 14(a). S11 Simulation of line width and plasma width variations.

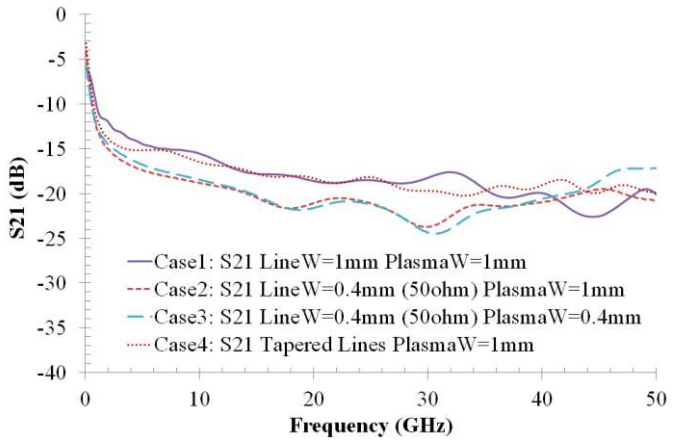

Fig. 14(b). S21 Simulation of line width and plasma width variations.

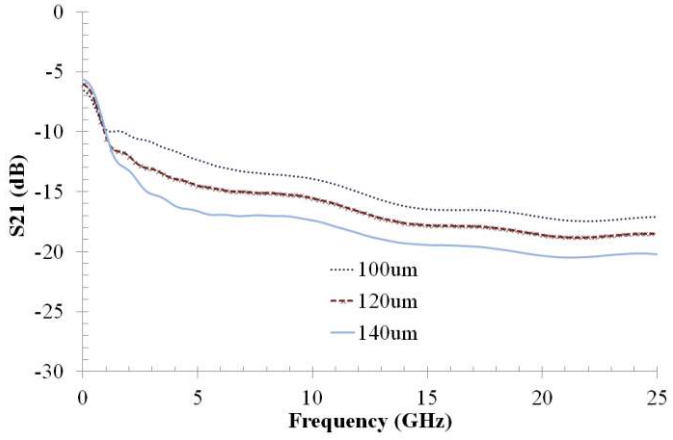

Fig. 15. Effect of varying diffusion length (Ld) for a 1 mm gap length.

Several other trends between simulation and measurement are shown in Fig. 16. A comparison between the multilayer layer and single layer results shows that at low frequencies the results are almost similar. However as frequency increases the single layer model deviates further from the results. This can be seen in Figs. 16a, b and c showing the comparison between single layer, multilayer and measured results at 1 GHz, 20 GHz and 40 GHz respectively. The conductivity values for the models were obtained from measured data (see Fig. 8). The deviation of the single layer model is particularly prominent for the 40 GHz case of Fig. 16c. The trends in the results remain closely matched between the multilayer model and the measured results.

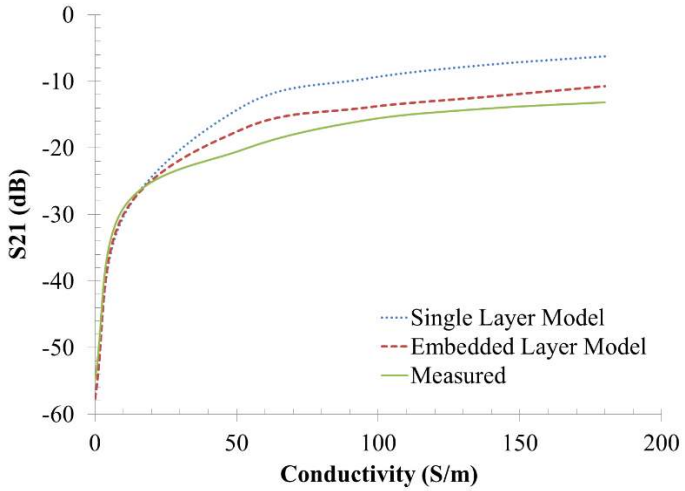

Fig. 16(a). Trends in S21 results at 1 GHz for varying conductivity/illumination levels.

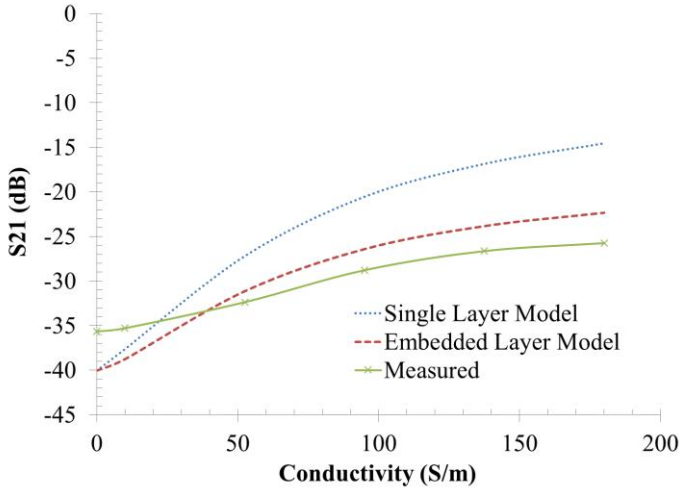

Fig. 16(b). Trends in S21 results at 20 GHz for varying conductivity levels.

These trends show that increases to conductivity do not automatically translate into improved attenuation for the measured case. This means that increases in conductivity are only effective if the plasma is better confined. The reasons for this are discussed in the next section relating to field distributions within the plasma.

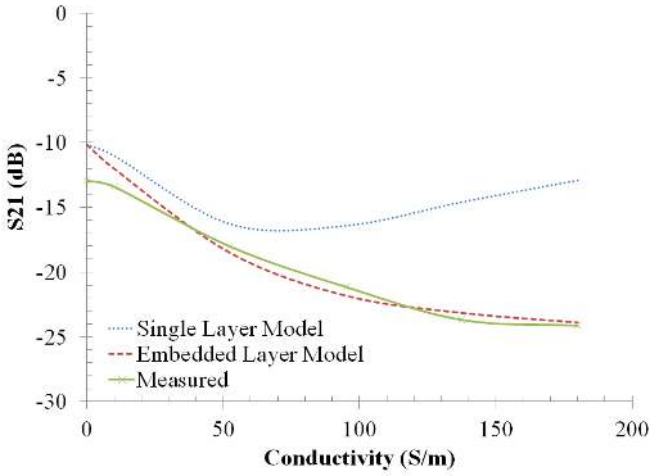

Fig. 16(c). Trends in S21 results at 40 GHz for varying conductivity levels.

C. Analysis Using Field Distributions

The differences in results between the single layer and multilayer models can be understood by considering the differences in the field distributions of each model. The fields in the multilayer model are pushed further toward the bottom layers of the plasma. This is unlike the single layer case where the position of the field maximum remains just below the plasma surface and does not change significantly with variations in conductivity or frequency. Figs. 17a and b show the Electric field distribution for each model through a planar cross-section of the plasma.

A plot of the E-Field vs. depth for the multilayer model at varying conductivity levels is shown in Fig. 18. This clearly shows the fields being pushed deeper into the substrate with increasing conductivity, which increases the fringing capacitance at the end of the microstrip line. This capacitance acts in parallel with the microstrip line [15] and forms the equivalent of a low pass filter. This accounts for the steep downward slope in the S_{21} of the multilayer model (Figs. 12 and 13) from between 45 MHz to about 2 GHz. At frequencies beyond this point the plasma length starts to become a significant portion of the microwave wavelength.

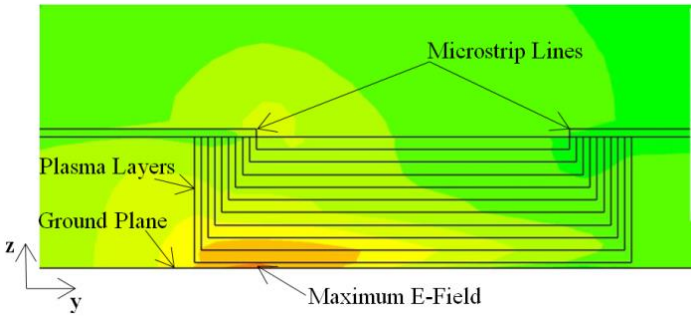

Figure 17(a): Multilayer model. Magnitude of E-Field (Magnitude) distribution across a Y-Z cross section of the plasma at 10 GHz

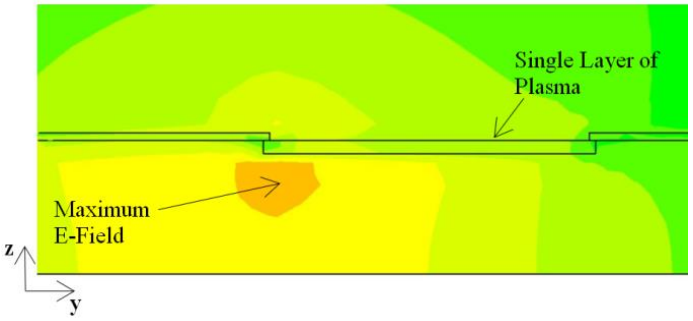

Fig. 17(b). Single Layer Model. E-Field (Magnitude) distribution across a Y-Z Cross Section of the plasma at 10 GHz.

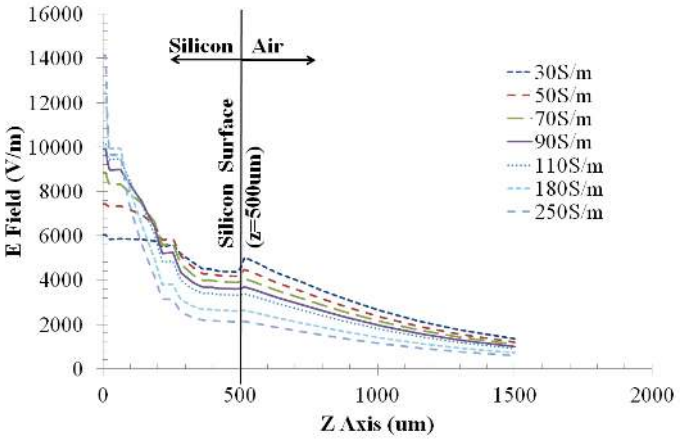

Fig. 18. E-field (Magnitude) distribution across the centre of the plasma for multilayer layer model in the z direction at 10 GHz.

The propagation of waves through such media has been studied theoretically [18]. This shows that for an inhomogeneously layered dielectric, a pure TEM mode cannot exist unless the direction of propagation of the incident wave is perpendicular to the surface of the layered medium. For all other cases the propagation must occur through a combination of TE and TM modes. For our layered dielectric shown in Fig. 17a, the perpendicular axis is in the z direction but the wave is incident from the y direction. Hence we expect multiple propagating modes through the plasma. However, since the diffusion profile is exponential, the top layers of the plasma is where the variation between individual layers is most significant and also where the conductivity is greatest. The variation in the bottom layers of the plasma is much less and hence can be approximated as being almost homogenous. The plasma region can then be split into two sections and each region analysed separately as shown below.

The TEM propagating mode in the bottom layers is considered first. The simulations showed this mode to exist in the lower layers of the plasma where the conductivity has decayed to well below the surface value but is still not zero. Fig. 19 shows a plot of the field contours at 10 GHz where E_z indicates the z component of the vector E-field. The propagation of this mode is similar to the propagation through a TEM transmission line containing a lossy dielectric. For the lower frequencies (below about 20 GHz) this is found to be the

dominant mode of propagation through the plasma. In this frequency range it can be seen that the E_z field is expelled from the top layers and hence the TEM mode is confined to the bottom layers. This can be approximated as a length of microstrip line with a thick upper conductor and containing a thin, lossy dielectric. The theory of propagation through such lossy media has been described in many textbooks [19].

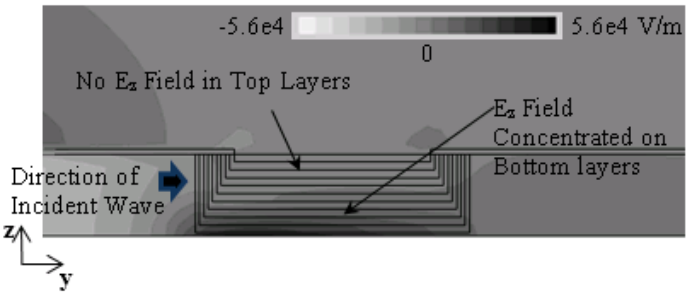

Fig. 19. Ez field contours for inhomogeneous multilayer plasma at 10 GHz this shows the TEM mode of propagation at the lower frequencies.

This can be applied here and used to explain the negative slope in the S_{21} of Fig. 13 from between 2 GHz to around 20 GHz. Although other components of the E field are present in the fringing field at the end of the microstrip line, these do not couple effectively into propagating modes and the TEM mode remains the dominant mechanism of transmission.

At frequencies above the 20 GHz range, the TEM mode of propagation is highly attenuated and is no longer the dominant propagating mode. Surface propagating modes and modes propagating in the higher layers of the plasma start to become equally dominant. The E_z field is also no longer confined to just the lower layers of the plasma and the approximation used for the 2 to 20 GHz range is no longer valid. This is thought to be the reason for the S_{21} graph in Fig. 12 not continuing to drop with the same slope after 20 GHz. The plot of E_z for 30 GHz is shown in Fig. 20 below.

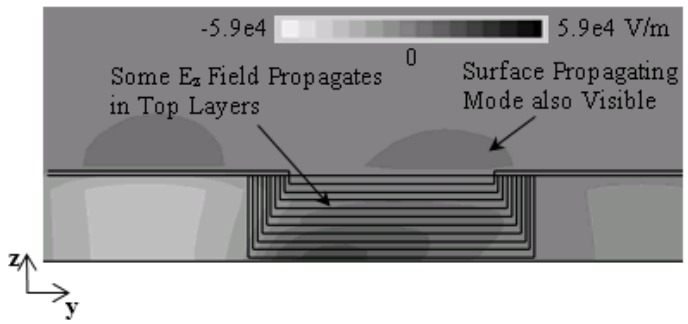

Fig. 20. Ez field contours for inhomogeneous multilayer plasma at 30 GHz. This shows the TEM mode along with some surface propagating modes.

A plot of the E_y field for 30 GHz (Fig. 21) shows that unlike at low frequencies, a significant amount of energy propagates via this field component and is nearly equivalent to a propagating TM mode. This component also undergoes attenuation due to the finite conductivity of the plasma layers.

From the analysis of the field plots we can conclude that the losses are mainly down to two factors, the finite conductivity in the top layers and the inhomogeneous decay caused by diffusion of the optically generated carriers. This decay is seen to be responsible for about 10dB of additional loss in transmission as shown in the comparisons with a single layer model (Fig. 13). It also means that the S_{21} characteristic at frequencies above 2 GHz would improve very little even with large increases to the conductivity.

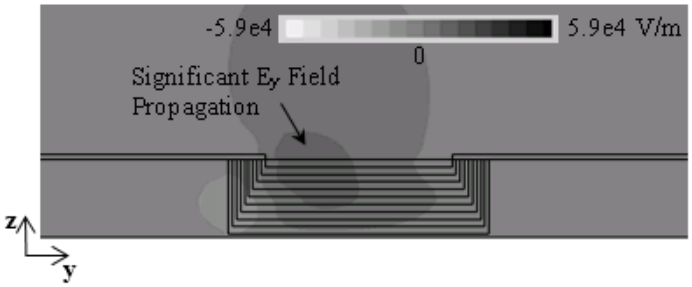

Fig. 21. Ey field contours for inhomogeneous multilayer plasma at 30 GHz. This shows a TMy propagating mode.

This is apparent from the trends in Figs. 16b and c and can also be seen from the measured data in Fig. 7. One method of recovering this loss is to confine the plasma to a thinner layer. While there are several methods for doing this, one method in particular seems to be quite promising and is currently being investigated. This is briefly outlined in the conclusion below.

V. Conclusion

The important characteristics of optically illuminated plasmas for microstrip structures have been highlighted. The rectangular multilayer model was seen to closely predict the measured microwave response of a microstrip gap up to about 20 GHz.

The attenuation caused by the exponential diffusion of the carriers was shown in detail. The effects of mismatch loss from a 30 Ω line impedance on the overall attenuation characteristics were investigated. The analysis of the field distribution allows the loss mechanisms to be clearly identified. The minimization of losses is important for applications where the plasma dimensions are a significant fraction of the microwave wavelength. We expect that considerable advantages in tuning can be achieved using long lengths of plasma which are reconfigurable by changes to the illumination pattern. We are currently investigating methods for minimizing losses by confining the plasma through the use of thin epitaxially grown layers on transparent substrates such as sapphire.

The conductivity vs. illumination graphs show that the conductivity limit in silicon has not yet been reached. This means that still higher conductivities can be achieved by increasing the illumination intensity. The conductivity can also be increased by coating the silicon surface with a passivation material. This has the effect of decreasing the surface recombination time. We are currently investigating the effectiveness of Plasma Enhanced Chemical Vapour Deposited

(PECVD) passivation surfaces such as silicon dioxide and silicon nitride.

We expect that the combinations of the above techniques along with the increasing miniaturization and power efficiency of infrared lasers will allow this type of illumination based tuning to compete with more established methods of microwave device tuning.

ACKNOWLEDGEMENTS

The authors would also like to extend special thanks to Dr. Maciej Klemm for help with running the CST simulations and to Dr. Andrew Murray for help with fabricating the samples.

REFERENCES

[1] D. S. Lockyer, J.C. Vardaxoglou, and M. J. Kearney, "Transmission through optically generated inductive grid arrays," IEEE Transactions on Microwave Theory and Techniques, vol. 47, no. 7, pp. 1391-1397, Jul. 1999.

[2] V.A. Manasson, L.S. Sadovnik, P.I. Shnitser, R. Mino, and J.S. Kruger; "Millimeter wave optically scanning antenna based on photoinduced plasma grating," SPIE Journal of Optical Engineering, vol. 35, no. 2, pp. 357-361, Aug. 1995.

[3] E.L. Khaldi, F. Podevin, and A. Vilcot, "An optically controlled continuous phase-shifter and magnitude controller on high-resistive silicon," Microwave and Optical Technology Letters vol. 38, no. 2, pp. 129-132, May 2003.

[4] J.K. Butler, Wu Tran-Fu, and M.W. Scott, "Nonuniform Layer Model of a Millimeter-Wave Phase Shifter," IEEE Transactions On Microwave Theory And Techniques, vol. 34, no. 1, pp. 147-155, Jan. 1986.

[5] C.H. Lee, P. S. Mak and A. P. Defonzo, "Optical control of millimeter-wave propagation in dielectric waveguides," IEEE Journal of Quantum Electronics, vol. 16, no. 3, pp. 277-288, Mar. 1980.

[6] B. Boyer, J. Haidar, A. Vilcot, and M. Bouthinon, "Tunable microwave load based on biased photoinduced plasma in silicon," IEEE Transactions On Microwave Theory And Techniques, vol. 45, no. 8, pp. 1362-1367, Aug. 1997.

[7] R. Gary, J.D. Arnould, and A. Vilcot, "Semi-analytical computation and 3D modeling of the microwave photo-induced load in CPW technology," Microwave and Optical Technology Letters, vol. 48, no. 9, pp. 1718-1721, Sept. 2006.

[8] C.D. Gamlath, D.M. Benton, and M.J. Cryan, "Microwave characterisation of optically illuminated silicon," in ICTON, 2012, pp. 1-4.

[9] C.D. Gamlath, D.M. Benton, and M.J. Cryan, "Investigation of an optically reconfigurable plasma for silicon based microwave applications," in EuMC, 2013, pp. 874-877.

[10] D. Naemen, Semiconductor Physics And Devices. 3rd ed., New York: McGraw-Hill, 2002.

[11] D.K. Schroder, "Carrier lifetimes in silicon," IEEE Transactions on Electron Devices, vol. 44, no. 1, pp. 160-170, Jan. 1997.

[12] S. Sze, Physics of semiconductor devices. 2nd ed., New York: Wiley, 1985.

[13] R. Gary, and A. Vilcot, "3D photo-induced load modeling for optically controlled microwave microstrip line," Microwave and Optical Technology Letters, vol. 40, no. 5, pp. 356- 359, Jan. 2004.

[14] R. Soares, Applications of Gallium Arsenide MESFETs. Dedham: Artech House, 1983, pp. 40-41.

[15] A. Bhadauria, A.K. Verma, E.K. Sharma, and B.R. Singh, "Optically controlled microstrip load and stub on silicon substrate," Microwave and Optical Technology Letters, vol. 39, no. 4, pp. 271- 276. Sep. 2003.

[16] Y. Horii, and M. Tsutsumi, "Scattering parameters of interdigital microstrip gap under laser spot illumination," in IEEE MTT-S International , 1997, pp. 8-13.

[17] R. W. Klopfenstein, "A transmission line taper of improved design," Proceedings of the IRE, vol. 44, no.1, pp. 31-35, Jan. 1956.

[18] W.C. Chew, Waves and fields in inhomogeneous media. vol. 522, New York: IEEE press, 1995.

[19] C.A. Balanis, Advanced engineering electromagnetics. 2nd ed., New York: Wiley, 2012, pp. 198-205.

Chris D. Gamlath received the BEng. degree with First Class Honours in Electronics and Communications engineering from the Robert Gordon University of Aberdeen, Scotland, U.K. in 2004 and the MSc. degree in electronic engineering from the University of Surrey at Guildford, U.K. in 2011. He is currently pursuing a Ph.D. degree in electrical and electronic engineering at the University of Bristol, U.K.

From 2004 to 2011 he was an RF Engineer working initially on offshore microwave telemetry systems and later on developing commercial RF-CMOS tuner ICs. His research interests include the investigation of microwave interactions with optically generated semiconductor plasmas and the use of this interaction for tuning microwave devices.

Professor Martin Cryan has been working in the fields of optical and microwave electromagnetic modelling, device and circuit fabrication and measurement for 27 years. He is a senior member of IEEE. Since 2000 he has worked in the area of nanophotonics and in particular photonic crystals and plasmonics.

He was appointed to a Lectureship in the department of electrical and electronic engineering at the University of Bristol and appointed as Professor of Applied Electromagnetics and Photonics in 2012. He has published 78 journal papers and more than 130 papers at international conferences.

Professor Cryan was the U.K. representative for URSI Commission D:Electronic and Photonics from 2011 to 2014.